Journal of Solid State Chemistry **164,** 326–331 (2002)
doi:10.1006/jssc.2001.9479, available online at http://www/idealibrary.com on IDEAL®

Magnetic and Mössbauer Study of the Novel $FeIn_2S_2Se_2$ Layered Compound

G. F. Goya,*[,1] A. Memo,† and H. Haeuseler†

*Instituto de Fisica, Universidade de São Paulo, CP 66318, 05389-970 SP, São Paulo, Brazil; †Laboratorium für Anorganische Chemie, Universität-Siegen, D-57068 Siegen, Germany

Received August 22, 2001; in revised form November 13, 2001; accepted December 3, 2001; published online February 11, 2002

The magnetic properties of the new polymorphic $FeIn_2S_2Se_2$ compound are presented. The system crystallizes in the α-$FeGa_2S_4$ structure at low temperatures, and undergoes a transition to a $MgAl_2S_4$-type structure at $T > 850°C$. For this high-temperature phase, low-field magnetization data show a peak at $T_1 = 12.5(5)$ K, below which magnetic irreversibility is observed. High-temperature susceptibility fits indicate the presence of antiferromagnetic interactions with a high degree of frustration. The effective magnetic moment $\mu_{eff} = 4.54(3)\ \mu_B$ agrees with the expected $3d^6$ ($S = 2$) configuration for Fe^{2+}. Mössbauer spectroscopy showed that Fe^{2+} ions are distributed in tetrahedral (A) and octahedral (B) sites with a $B{:}A \approx 1$ ratio. The ac susceptibility data were analyzed according to conventional power law dynamics, giving a freezing temperature $T_g = 12.5(2)$ K and critical exponent $z\nu = 6.5 \pm 1$, in agreement with Monte Carlo simulations for 3D short-range Ising spin–glass systems. © 2002 Elsevier Science (USA)

Key Words: **layered materials; selenides; spin glass; mössbauer spectroscopy; $FeIn_2S_2Se_2$.**

INTRODUCTION

Chalcogenides with the composition AB_2X_4 (A,B = transition metal and X = chalcogen atom) have long attracted attention due to their magnetic and magneto-optic properties (1, 2). In particular, thiospinels AB_2S_4 have been revisited recently since they show a metal-to-insulator transition at high pressure, and the ability to form both metallic and insulating spin glasses (3–7). The solid solutions $AB_2(S_{1-x}Se_x)_4$ usually crystallize in layered structures, attributed to the enhanced preference for tetrahedral coordination with increasing selenium contents. At the other end of the series, the selenides are less known regarding their crystal and magnetic structures. Recently, the $FeIn_2(S_{1-x}Se_x)_4$ solid solution has been obtained for $0 \le x \le 1$, and different structures have been reported, depending on the x value (8). The spinel structure is observed within compositions $0 \le x \le 0.25$, whereas a polymorphic transition from α-$FeGa_2S_4$ to $MgAl_2S_4$ structures is found for $0.4 \le x \le 0.55$ (low- and high-temperature phases, respectively). The obtained phase diagram shows that the phase boundaries are almost temperature independent.

The crystal lattices of these sulfides and selenides can be locally nonstoichiometric due to the presence of vacancies, breaking the superexchange paths between magnetic ions and thus resulting in magnetic frustration and spin–glass (SG) transition at low temperatures. Whereas evidence of a SG transition can be obtained from the critical parameters from scaling of the magnetization and/or susceptibility curves, ^{57}Fe Mössbauer spectroscopy (MS) provides a suitable tool to sense minute changes in the local electric field gradient (EFG) and magnetic field at the Fe nucleus. We present in this work a characterization of the hyperfine and magnetic properties of the $FeIn_2S_2Se_2$ compound with $MgAl_2S_4$ structure, using Mössbauer spectroscopy, ac susceptibility, and dc magnetization.

EXPERIMENTAL PROCEDURE

The material was prepared by sintering stoichiometric mixtures of the binary sulfides in evacuated and sealed silica ampoules at 600°C. To obtain the desired high-temperature phase, samples were quenched from 900°C to room temperature, as described elsewhere (8). Structural studies of the powdered products were made by powder X-ray diffraction and Guiner radiographs. Diffraction patterns were refined using the Rietveld method to extract structural data. Mössbauer spectra were recorded in transmission geometry between 4.2 K and 300 K using a ^{57}Co/Rh matrix source in constant acceleration mode, using a nonlinear least-squares program to fit the spectra to Lorentzian line shapes. Isomer shifts are referred to α-Fe at 300 K. To perform magnetic measurements, small crystallites of the samples were dispersed in epoxy resin, and

[1]To whom correspondence should be addressed. Fax: (55)11 3818 6984. E-mail: goya@macbeth.if.usp.br.

0022-4596/02 $35.00

molded in cylindrical shape of diameter = 5 mm and height = 3 mm. Magnetization measurements were performed in a commercial superconducting quantum interference device (SQUID) magnetometer in both zero-field-cooling (ZFC) and field-cooling (FC) modes, between $5\,K \leq T \leq 300\,K$ and applied fields up to 70 kOe. The diamagnetic contribution of the sample holder was subtracted, and the resulting susceptibilities were further corrected for core diamagnetism of the ions. Ac susceptibility data were taken in $\Delta T \sim 0.05$ K steps and measuring times ~ 10 min at each point to determine the transition temperature. To study the frequency-dependent cusp of the absorptive $\chi'(T)$ and dispersive $\chi''(T)$ components of the ac magnetic susceptibility, data were taken using driving fields in the $10\,mHz < f \leq 1.1$ kHz range, with amplitude of 1 Oe.

EXPERIMENTAL RESULTS

Structural parameters obtained from Rietveld refinement were reported previously (8), and are reproduced in Table 1 for clarity. The structure of this compound can be described in terms of slabs formed by four anion layers, stacked in the *c*-axis direction and separated from each other by a van der Waals gap (9). These slabs are in turn composed by a central layer of octahedra surrounded by two sheets of tetrahedra. The change from the low- to high-temperature phase yields slight compression and enlargement of octahedral and tetrahedral sites, respectively, maintaining the total volume of the slabs (and the basal *a* cell parameter) unchanged. Some hints pointing to disorder of the anion sublattice at high temperatures could also be obtained from the X-ray patterns, but the polycrystalline nature of the sample prevents a definite conclusion.

TABLE 1
Refined Atomic Parameters, Site Occupation Factors (*sof*), and Selected Interatomic Distances and Angles for $FeIn_2S_2Se_2$ with $MgAl_2S_4$-Type Structure[a]

Atom	Site	*x*	*y*	*z*	sof
Fe1	3*a*	0	0	0	0.56
In1	3*a*	0	0	0	0.44
Fe2	6*c*	0	0	0.2344(6)	0.22
In2	6*c*	0	0	0.2344(6)	0.78
S1	6*c*	0	0	0.1274(9)	0.5
Se1	6*c*	0	0	0.1274(9)	0.5
S2	6*c*	0	0	0.2982(9)	0.5
Se2	6*c*	0	0	0.2982(9)	0.5

Bond	Distance (Å)
M_{Tet}–S(1)/Se(1)	2.523(5)
M_{Tet}–S(2)/Se(2)	2.450(6)
M_{Oct}–S(2)/Se(2)	2.644(5)

Bond	Angle (°)
S(1)/Se(1)–M_{Tet}–S(1)/Se(1)	102.6(5)
S(1)/Se(1)–M_{Tet}–S(2)/Se(2)	115.7(5)
S(2)/Se(2)–M_{Oct}–S(2)/Se(2)	96.3(4)
S(2)/Se(2)–M_{Oct}–S(2)/Se(2)	83.7(4)

[a]Space group $R\bar{3}m$, $Z = 3$, lattice parameters $a = 3.9383(8)$ Å and $c = 38.395(9)$ Å.

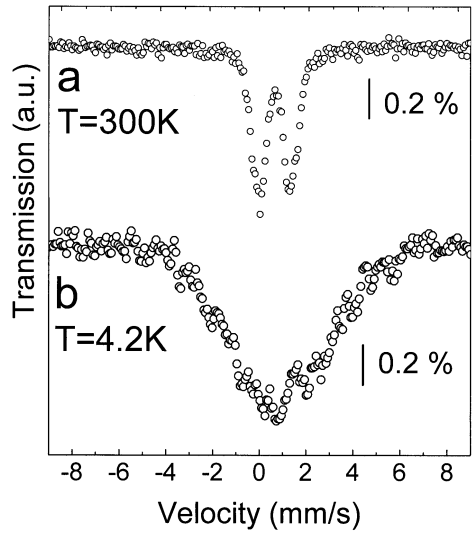

FIG. 1. High-velocity Mössbauer spectra for the $MgAl_2S_4$-type phase of $FeIn_2S_2Se_2$, taken at (a) room temperature and (b) 4.2 K.

Room temperature Mössbauer spectra taken in high-velocity scale showed the presence of one central doublet, without magnetic phases present (Fig. 1a). The Mössbauer spectrum taken at 4.2 K (Fig. 1b) shows broad unresolved lines due to relaxation effects, indicating that magnetic order is not complete at this temperature. To fit the central doublet, Mössbauer spectra were taken in a low-velocity scale, as shown in Fig. 2. The fitting of this spectrum was done using two doublets and one single line having hyperfine parameters shown in Table 2. The isomer shift

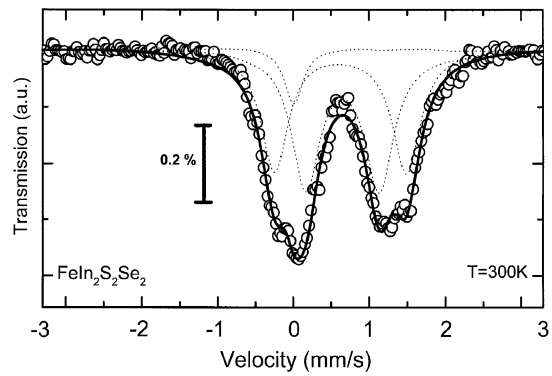

FIG. 2. Low-velocity Mössbauer spectrum at room temperature. Three components (dotted lines) were used to make a fit (solid line) of experimental data (open circles).

TABLE 2
Hyperfine Parameters from Mössbauer Spectra of $FeIn_2Cr_2S_2Se_2$ at Room Temperature: Quadrupolar Splitting (ΔQ), Isomer Shift (δ), Line Width (Γ), and Relative Spectral Area (A)[a]

Site	ΔQ (mm/s)	IS (mm/s)	Γ(mm/s)	Area (%)
DQ1	0.94(2)	0.78(1)	0.44(2)	44(3)
DQ2	1.70(2)	0.73(1)	0.50(2)	52(3)
L1	—	0.09(2)	0.28(4)	4(3)

[a]Errors are given in parentheses.

values for the two doublets are consistent with those expected for an Fe^{2+} oxidation state. Partial covalent character of the Fe–Se bonding may account for the small difference between our $IS \approx 0.7$ mm/s and the $IS \sim 0.8$–1.0 mm/s values usually found in ionic compounds containing Fe^{2+}. It can be noticed that the ratio of spectral areas between the two doublets (i.e., between iron populations at each site) is close to 1, indicating that the population at these sites is different from the other known polytypes of the series (10). Our assignment of the two doublets was based on the expected symmetry for each site. Whereas a $\Delta Q = 0$ value should be expected for a nondistorted site with cubic symmetry, crystallographic data in Table 1 show that both M_{Tet} and M_{Oct} coordination polyhedra are distorted from their "perfect" symmetry, creating an electric field gradient at Fe nuclei and thus nonzero values of ΔQ. The random distributions of S and Se are also likely to contribute to the observed electric field gradient. It is well known that in both iron oxides and chalcogenides the rule of thumb $\Delta Q(Fe^{2+})_{Tet} > \Delta Q(Fe^{2+})_{Oct}$ can be applied (11), where the subscripts Tet and Oct stand for tetrahedral and octahedral coordination of Fe, respectively. Thus, we assign the higher ΔQ_1 value to tetrahedrally coordinated Fe^{2+} in the structure, and the lower ΔQ_2 to octahedral sites. The spectrum shows, in addition, a single line amounting to $\sim 4 \pm 1\%$ of the total resonant area with hyperfine parameters corresponding to non-magnetic nanometer-size γ-Fe (fcc) particles. This assignment is based on the observation of the same line in Mössbauer spectra of $FeIn_2Se_4$ and (low-T phase) $FeIn_2S_2Se_2$ samples, at temperatures down to 4.2 K. Previous experimental and theoretical works on fcc-Fe have shown that, due to the volume dependence of the ground state, nanosized γ-Fe particles are paramagnetic down to 1.8 K (12). The presence of this phase seems to originate from the reduction of the starting sulfide.

ZFC–FC magnetization curves taken at low field are shown in Fig. 3. A sharp transition is observed at $T_1 = 12.5(5)$ K, and below this point the FC and ZFC branches display irreversible behavior similar to that of iron-containing thiospinels (13). Magnetization curves in

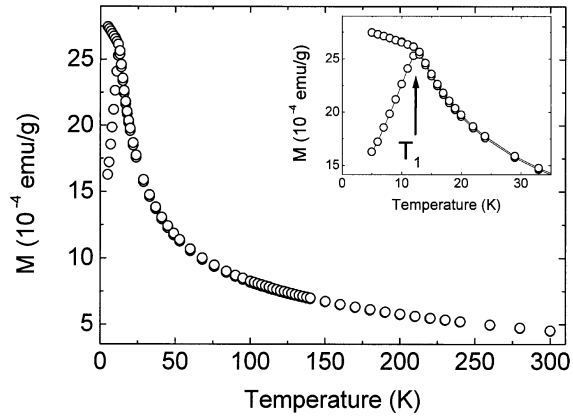

FIG. 3. FC-ZFC magnetization curves with applied field of $H_{app} = 5$ Oe. Inset: amplification of the low-T region showing the transition at $T \sim T_1$.

ZFC–FC modes taken at higher applied fields (Fig. 4) show that the temperature T_1 of the irreversible point (defined as the point where FC and ZFC branches separate) steadily shifts to lower values with increasing field, attaining $\sim 7 \pm 1$ K for $H = 70$ kOe. No significant changes are observed in the paramagnetic (PM) regime with increasing fields. In the PM region, the M/H (labeled as χ_{dc}) vs T curves were found to obey a Curie–Weiss law $\chi_{dc} = C/(T-\Theta)$. From the fit of χ_{dc} in the $T > 100$ K range (inset of Fig. 4), we obtained $\Theta = -126(3)$ K for the Weiss temperature and $\mu_{eff} = 4.54(3)\ \mu_B$ for the effective magnetic moment, similar to those previously reported for $FeIn_2S_4$ (14). This similarity between Curie-Weiss parameters in $FeIn_2S_2Se_2$ and $FeIn_2S_4$ ($-126(3)$ K and $-122(3)$ K in Ref. (14), respectively) suggests that the effective superexchange interactions involves mainly Fe–S paths. The μ_{eff} value is about 10% smaller than expected for the free ion value ($Fe^{2+} \sim 4.9\ \mu_B$), which might be due to covalence effects.

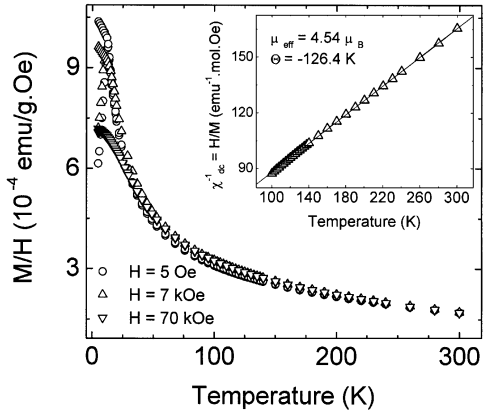

FIG. 4. FC-ZFC magnetization curves taken at different applied fields. Inset: molar dc susceptibility $\chi_{dc} = M/H$ in the paramagnetic region. The solid line is the best fit using a Curie–Weiss law $\chi = C/(T-\Theta)$.

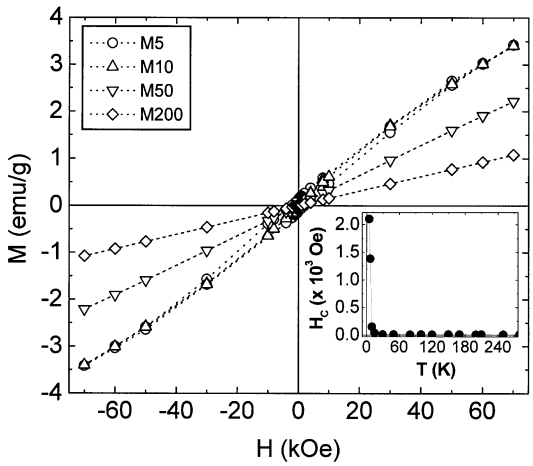

FIG. 5. Magnetization curves vs applied field at selected temperatures. The inset shows the low-field region, where a coercive field H_C develops for $T < T_1$.

Additionally, from the C value reported in Ref. (14) an effective magnetic moment $\mu_{eff} = 4.85\,\mu_B$ is deduced, which lies between the free-ion value and our result for $FeIn_2S_2Se_2$, as could be expected from a simple picture based on the electronegativity differences in S–Fe and Se–Fe chemical bonds. Magnetization vs applied field cycles performed at different temperatures (Fig. 5) show PM behavior for temperatures $T > T_1$. For $T < T_1$, the sudden appearance of a coercive field H_C is observed, in agreement with the irreversibility in ZFC–FC curves. The value of coercive field at 5 K, namely $H_C = 2.1(1)$ kOe, is considerably larger than the values usually found in sulfides and selenides (2, 15).

Figure 6 shows the real $\chi(T)$ and the imaginary $\chi''(T)$ components of the ac susceptibility at some selected frequencies. For temperatures $T \geq 20$ K, the in-phase $\chi'(T)$ and out-of-phase $\chi''(T)$ components overlap for the different frequencies, indicating that the system is in thermodynamic equilibrium. For lower temperatures, it can be observed that, at each frequency, the temperature T_f of the maximum in the absorption component χ' is almost coincident with the inflection point observed in the dispersion component χ''. It can be also noticed from Fig. 6 that the peak of the real component broadens as it shifts to higher T for higher applied frequencies.

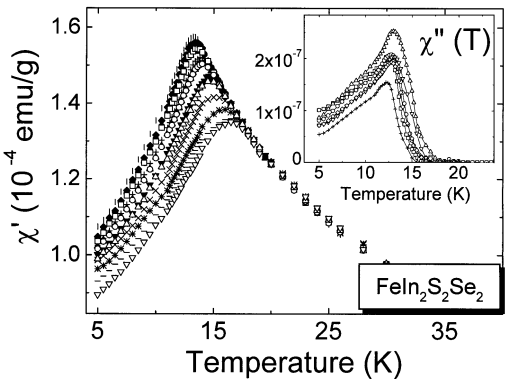

FIG. 6. Ac susceptibility data taken at different driving frequencies, showing the shift of the temperature of the maximum. The excitation field was $H = 2$ G. The driving frequency were between ~ 10 mHz and ~ 1.12 kHz.

DISCUSSION

From the inspection of the structural data presented in Table 1 it can be inferred that, since the unit cell has $c \sim 10a$ and the layers of M_{Oct}/M_{Tet} sites are parallel to the ab planes, there is a considerable separation between layers. Within each layer, the exchange paths connecting M_{Tet} to M_{Oct} cations are essentially those involving one S(2) or Se(2) anion, whereas the shortest M_{Tet}–M_{Tet} exchange path (within the same or at different layers) must involve at least two S(1) (or Se(1)) anions. It is interesting to note that, as a consequence of this layered structure, low-dimensional magnetic properties could be expected. However, no evidence of $D < 3$ magnetic order can be observed from the $M(T)$ curves between 5 K and 300 K, which approximately follow a Curie–Weiss regime down to $T \approx 1.5\,T_1$. The existence of anisotropy effects, on the other hand, is difficult to establish due to the polycrystalline nature of the present samples.

For a SG state to develop, it is usually assumed that some degree of magnetic frustration is needed, either from competing interactions or randomness of spin positions. The small ratio $T_1/\Theta \approx 0.1$ between the transition temperature and the Curie–Weiss parameter (which is a measure of the exchange interactions in the system) indicates that a large degree of frustration is indeed present in $FeIn_2S_2Se_2$. This frustration probably originates in the randomness of spin positions as the Fe ions are statistically distributed over the tetrahedral and octahedral sites. It is worth noting that ordering of the Fe atoms would result in a different space group.

The frequency-dependent cusp of ac data agrees with the existence of a frozen state below ~ 14 K. To analyze whether this corresponds to a true SG transition is not a trivial task, because even the nature of the SG phase is still matter of discussion (16,17). The usual way to obtain quantitative evidence for spin–glass behavior is from the relative shift of the temperature of the maximum, T_m, in the real component of the ac susceptibility $\chi'(T)$, through the relationship

$$W = \Delta T_m / (T_m \Delta \log(\omega)) = 4.7 \times 10^{-2}. \qquad [1]$$

Although this value is larger than the (5–9) $\times 10^{-3}$ found in canonical spin–glasses such as MnCu and AuFe (18), it is much smaller than the shift in a superparamagnet (19).

Interestingly, a similar value $W = 6 \times 10^{-2}$ has been reported for several members of the $(Eu_{1-x}Sr_x)S$ family of insulating spin–glasses (20).

We have tried two different approaches in the analysis of the frequency dependence to clarify the underlying physical mechanism. The activated dynamics model for critical behavior in disordered systems assumes the existence of free-energy barriers for relaxation processes, giving relaxation times that follow a Vogel–Fulcher law,

$$f = f_0 \exp[E_A/(T - T_0)], \quad [2]$$

where f is the applied frequency, E_A is the activation energy, and T_0 is a measure of the interactions between particles (or clusters). Applying this relationship yielded the unrealistic 9.8(2) K and 51(5) K values for T_0 and E_A, respectively, indicating that this model is not appropriate to describe the present system.

A second determination of the SG parameters was based on the conventional critical slowing down for relaxation of the magnetic moments, valid for a SG phase transition at finite temperature. From the theory of dynamical scaling near a phase transition it is known that the divergence of the relaxation time τ when approaching the freezing temperature from above, is described by the relation

$$f = f_0 t^{z\nu}, \quad [3]$$

where $t = (T_f - T_g)/T_g$ is the reduced temperature, T_f is the freezing temperature at each frequency, T_g is the SG transition temperature, and zv is a dynamic critical exponent. Typical values for f_0 are in the 10^{12-13} Hz range for canonical spin–glasses, such as CuMn and AuMn. We note here that the frequently used criteria to extract the freezing temperatures T_f at different frequencies, e.g., the χ' or χ'' maximum, yields incorrect results since they define sets of T_f (H, ω) values for which τ is not necessarily constant. Instead, we have used a criterion (21) that involves the quantity

$$\tan\phi = \chi''/\chi' = \omega\tau, \quad [4]$$

setting $\tan\phi \sim \phi =$ constant, where the constant value was chosen to be small compared to the value at the inflection point. This defines a set of T_f values that satisfy the $\omega\tau =$ constant condition. As shown in Fig. 7, the T_f values defined in this way yield the expected linear dependence of log t vs log f, and the best fit is obtained with $f_0 = 1.96 \times 10^6$ Hz, $T_g = 12.5(2)$ K, and $zv = 6.5 \pm 1.0$. The resulting value of the dynamic critical exponent zv is similar to previous results found for other 3D short-range Ising spin glasses (22, 23). From the theoretical side, Monte Carlo simulations of the Ising system ($\pm J$ model), assuming that $T_g = 0$ for the SG–PM transition, yielded $zv = 4$ for the three-dimensional case and $zv = 2$ for two dimensions (24). On the other side, Monte Carlo simulations of short-range Ising spin–glass (discrete nearest-neighbor $\pm J$ model in a 3D cubic lattice) have shown that zv can vary from 5.5 ± 0.5 to 7.2 ± 0.8 depending on the different methods of analysis (25). Our results show clearly that the latter model with $T_g > 0$ is more appropriate to describe the SG transition in $FeIn_2S_2Se_2$.

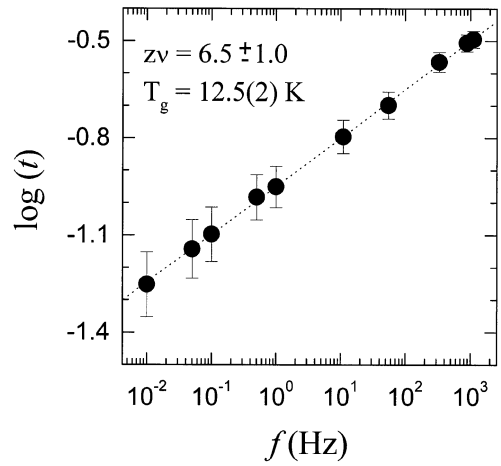

FIG. 7. Plot of T_g vs ac driving frequency f. The dotted line is the best fit to the experimental points using Eq. [1].

CONCLUSIONS

The magnetic characterization of the high-temperature polytype $FeIn_2S_2Se_2$ has been accomplished. Antiferromagnetic interactions were found in the paramagnetic regime, yielding a magnetic transition from the PM to an ordered state at $T_1 = 12.5(5)$ K. Despite its layered structure, the magnetic behavior was determined to be of three-dimensional type. Partial inversion of the cations was determined from the resonant areas at room temperature. From ac susceptibility data at different frequencies, a spin–glass transition has been found to occur at $T \approx 14$ K. The critical parameter $zv = 6.5 \pm 1.0$ resulting from the conventional critical slowing down fits of $\chi'(T)$ and $\chi''(T)$ indicates that this system is well described by a 3D short-range Ising spin–glass model.

ACKNOWLEDGMENTS

G.F.G. acknowledges financial support from Fundação de Amparo à Pesquisa do Estado de São Paulo (FAPESP). H.H. and A.M. are grateful to the Deutsche Forschungsgemeinschaft (DFG) for financial support of this research.

REFERENCES

1. P. K. Baltzer, H. W. Lehmann, and M. Robbins, *Phys. Rev. Lett.* **15,** 493 (1965).
2. R. P. van Stapele, *in* "Ferromagnetic Materials" (E. P. Wohlfarth, Ed.), Vol. 3, Chap. 8. North-Holland, Amsterdam, 1982.

3. J. Tang, T. Matsumoto, T. Furubayashi, T. Kosaka, S. Nagata, and Y. Kato, *J. Magn. Magn. Mater*. **177–181,** 1363 (1998).
4. S. Nagata, N. Matsumoto, Y. Kato, T. Furubayashi, T. Matsumoto, J. P. Sanchez, and P. Vulliet, *Phys. Rev. B* **58,** 6844 (1998).
5. M. Muroi, R. Street, and P. G. McCormick, *Phys. Rev. B* **63,** doi: 052412/prb.2001.
6. M. S. Park, S. K. Kwon, S. J. Youn, and B. I. Min, *Phys. Rev. B* **59,** 10018 (1999).
7. Lubecka, L.J. Maksymowicz, R. Szymczak, and W. Powroznika, *J. Magn. Magn. Mater*. **177,** 97–98 (1998).
8. S. Reil and H. Haeuseler, *J. Alloys Comp*. **270,** 83 (1998).
9. H. Haeuseler and S. K. Srivastava, *Z. Kristallogr*. **215,** 205 (2000).
10. K. G. Nikiforov, *Prog. Cryst. Growth Charact. Mater*. **39,** 1 (1999).
11. N. N. Greenwood and T. C. Gibb, "Mössbauer Spectroscopy." Chapman & Hall, London, 1971.
12. G. Goya, A. Memo, and H. Haeuseler, to be published. For the magnetic properties of γ-Fe nanoparticles, see: K. Haneda, Z. X. Zhou, A. H. Morrish, T. Majima, and T. Miyahara, *Phys. Rev. B* **46,** 13832 (1992).
13. G. F. Goya, H. R. Rechenberg, and V. Sagredo, *J. Magn. Magn. Mater*. **226,** 1298 (2001). See also: L. Brossard, J. L. Dormann, L. Goldstein, P. Gibart, and P. Renaudin, *Phys. Rev. B* **20,** 2933 (1979).
14. M. Eibchüz, E. Hermon, and S. Shtrikman, *Solid. State. Commun*. **5,** 529 (1967).
15. K. Binder and A. P. Young, *Rev. Mod. Phys*. **58,** 802 (1986).
16. Y. Ozeki and N. Ito, *Phys. Rev. B* **64,** doi: 024416/prb.2001.
17. H. G. Ballesteros, A. Cruz, L. A. Fernández, V. Martín-Mayor, J. Pech, J. J. Ruiz-Lorenzo, A. Tarancón, P. Téllez, C. L. Ullod, and C. Ungil, *Phys. Rev. B* **62,** 14237 (2000).
18. E. Agostinelli, D. Fiorani and A. M. Testa, "Fundamental and Applicative Aspects of Disordered Magnetism," p. 30. World Scientific Co., Singapore, 1987.
19. J. I. Gittleman, B. Abeles and S. Bozowski, *Phys. Rev. B* **9,** 3891 (1974).
20. J. A. Mydosh, "Spin Glasses," Chap. 3. London, 1993. Taylor & Francis.
21. N. Bontemps, J. Rajchenbach, R. V. Chamberlin, and R. Orbach, *Phys. Rev. B* **30,** 6514 (1984).
22. A. Sundaresan, A. Maignan, and B. Raveau, *Phys. Rev. B* **56,** 5092 (1997).
23. K. H. Fischer and Jertz, "Spin Glasses." Cambridge Univ. Press, Cambridge, 1991.
24. K. Binder and A. P. Young, *Phys. Rev. B* **29,** 2864 (1984).
25. A. T. Ogielski, *Phys. Rev. B* **32,** 7384 (1985).